described (*10*). Membranes were incubated for 1 hour with Dcytb antisera (antiserum 836) at a dilution of 1:100. Detection of the primary antibody was performed with the Westernbreeze system (Invitrogen). For immunohistochemistry, sections (5 μm) were cut from frozen tissue blocks at −20°C and placed on glass slides, fixed for 10 min at room temperature in acetone, and allowed to air-dry. Blocking was performed in 1% bovine serum albumin in phosphate-buffered saline (PBS) for 30 min. Sections were incubated with primary Dcytb antibody (antiserum 834) diluted 1:100 for 1 hour in blocking buffer. After extensive washing in PBS, sections were incubated for 30 min with a fluorescein isothiocyanate (FITC)–conjugated anti-rabbit secondary (DAKO, Carpinteria, CA) and then washed extensively with PBS. Sections were counterstained with propidium iodide and mounted. Images were captured on an MRC1024 confocal microscope (Bio-Rad). As a negative control, we processed parallel sections incubated with preimmune sera in the same way. No signal was obtained with preimmune serum.

19. R. J. Simpson, *J. Nutr.* **126**, 1858 (1996).
20. F. R. DeLeo *et al.*, *J. Lab. Clin. Med.* **134**, 275 (1999).
21. D. K. O'Riordan *et al.*, *Eur. J. Clin. Invest.* **25**, 722 (1995).
22. D. Trinder *et al.*, *Gut* **46**, 270 (2000).
23. *Xenopus* oocytes were prepared for injection as previously described (*5*). To synthesize Dcytb cRNA, we linearized the mouse Dcytb/pcDNA3.1 construct with Avr II and cRNA transcribed from the T7 RNA polymerase promoter site, using a commercial kit (Ambion, Austin, TX). Oocytes were injected with 25 ng of cRNA. Controls were injected with the same volume of water or 25 ng of an unrelated cRNA encoding a membrane protein. Reductase assays were carried out on individual oocytes 48 hours after injection. Oocytes were incubated for 10 hours in the dark in 50 μl of either standard Barths solution (pH 7.4) or buffer ND96 [98 mM NaCl, 2.0 mM KCl, 0.6 mM $CaCl_2$, 1.0 mM $MgCl_2$, and 10 mM Hepes (pH 6.0), with tris base] containing 100 μM $FeNTA_2$ (100 μM ferric chloride: 200 μM nitrilotriacetic acid) and 1 mM ferrozine. Formation of ferrous iron was calculated by measuring the optical density of the oocyte incubation buffer at 562 nm. Results were consistent in experiments performed on batches of oocytes harvested from three individual frogs. HuTu-80 and CaCo-2 cells were obtained from the American Type Culture Collection. Both cell types were cultured in Dulbecco's modified Eagle's medium (Sigma) containing 10% fetal calf serum and antibiotics [penicillin G (3 mg/liter) and streptomycin (5 mg/liter)] supplemented with nonessential amino acids (Sigma). Human Dcytb was excised from the original vector [pME18S-FL/Dcytb (GenBank accession number AK027115)] with Eco RI and Xho I and subcloned into the pcDNA3.1myc/his(+) mammalian expression vector (Invitrogen). Cells grown to ~40% confluence in 10-cm plates were transfected with ~2 μg of DNA, using the transfection reagent Effectene, following manufacturer's instructions (Qiagen, Valencia, CA). Stable cell lines were obtained by selection in G418 sulfate (50 μg/ml) (Calbiochem, Darmstrad, Germany) for 10 days. Expression of Dcytb was confirmed by Western blotting. The MTT assay is based on the reduction of a yellow, water-soluble monotetrazolium salt, MTT, to an insoluble purple formazan. HuTu-80 cells (mixed population of Dcytb-expressing cells and untransfected cells) were seeded in 96-well plates (1×10^4/ml) and left to grow for 48 hours. On the day of the assay, the medium was removed, and cells were incubated with Dcytb antibody (834 antiserum) in PBS or with PBS alone for 15 min. Solutions were removed and replaced with culture medium containing 20 μl of MTT solution (5 mg/ml) and incubated at 37°C for varying times. The medium and MTT solution were then removed, and 200 μl of dimethyl sulfoxide was added to each well. Absorbance was read at 540 nm. Data are the average of six wells, and the experiment was repeated three times with similar results. Ferric reductase assays were carried out on CaCo-2 cells as follows. Cells were harvested and homogenized in PBS with a glass Dounce-type homogenizer and centrifuged for 10 min at 10,000*g* to remove mitochondria, nuclei, and intact cells. The supernatant (corresponding to microsomes, plasma membrane, and cytosol) was incubated with 10 μM NADH in 50 mM Hepes (pH 7.4) with 100 μM $FeNTA_2$ and 1 mM bathophenanthroline at 37°C for up to 2 hours. Absorbance was read at 540 nm versus blanks lacking cells. For antibody-blocking experiments, cells were preincubated for 15 min at room temperature with antibody to Dcytb (834 antiserum diluted 1:50). The experiment shown was representative and has been repeated with the same result. For NBT assays, the duodenum was removed, opened lengthwise, and rinsed with 150 mM NaCl. Slices (full width of duodenum by 1 to 2 mm) were taken ~1 cm from the pylorus and incubated for 5 min at 37°C in 200 μl of 1 mM NBT in incubation buffer [125 mM NaCl, 3.5 mM KCl, and 16 mM Hepes/NaOH (pH 7.4)]. After incubation, tissues were rinsed twice with 150 mM NaCl and photographed with a Polaroid Microcam and a dissecting microscope. Inhibition of NBT reductase was demonstrated by preincubation of the tissue for 15 min with 200 μl of preimmune or antiserum to Dcytb (834 antiserum diluted 1:100 in incubation buffer), rinsing once in 200 μl of incubation buffer, then incubating and washing as above. The experiment shown was representative of at least three similar results. The mouse Dcytb construct used in oocyte experiments began MEGYRG, whereas in later experiments in cultured cells, we used a human Dcytb construct, which started MAMEGYRG (*28*). Both constructs induced reductase activity in transfected cells and gave a 30-kD protein by Western blotting. We do not at present know which methionine is used as the start of translation.
24. R. J. Simpson *et al.*, *Clin. Sci.* **96**, 16P (1999).
25. E. Georgatsou, D. Alexandraki, *Mol. Cell. Biol.* **14**, 3065 (1994).
26. D. G. Roman *et al.*, *Mol. Cell. Biol.* **13**, 4342 (1993).
27. K. Kobayashi, M. Tsubaki, S. Tagawa, *J. Biol. Chem.* **273**, 16038 (1998).
28. Single-letter abbreviations for the amino acid residues are as follows: A, Ala; C, Cys; D, Asp; E, Glu; F, Phe; G, Gly; H, His; I, Ile; K, Lys; L, Leu; M, Met; N, Asn; P, Pro; Q, Gln; R, Arg; S, Ser; T, Thr; V, Val; W, Trp; and Y, Tyr.
29. R. J. Simpson, T. J. Peters, *Biochim. Biophys. Acta* **772**, 220 (1984).
30. This work was supported by a Medical Research Council Training Fellowship (A.T.M.) and by the Wellcome Trust. The authors gratefully acknowledge the Joint Research Committee of King's College Hospital (D. Barrow), the Personal Assurance Charitable Trust (A.B.), the Royal Society (UK) (G.O.L.-D.), and the government of Libya (G.S.) for additional support. The authors thank A. Pini and R. Hider for support and encouragement and acknowledge C. Gove, J. Pizzey, and C. McNulty (Randall Institute, King's College London) for assistance in performing in situ hybridizations and U. Berger and N. Basora (Harvard Medical School) for advice and assistance with immunohistochemistry.

6 November 2000; accepted 19 January 2001
Published online 1 February 2001;
10.1126/science.1057206
Include this information when citing this paper.

Spins in the Vortices of a High-Temperature Superconductor

B. Lake,[1] G. Aeppli,[2,3]* K. N. Clausen,[3] D. F. McMorrow,[3] K. Lefmann,[3] N. E. Hussey,[4,5]† N. Mangkorntong,[4] M. Nohara,[4] H. Takagi,[4] T. E. Mason,[1] A. Schröder[6]

Neutron scattering is used to characterize the magnetism of the vortices for the optimally doped high-temperature superconductor $La_{2-x}Sr_xCuO_4$ ($x = 0.163$) in an applied magnetic field. As temperature is reduced, low-frequency spin fluctuations first disappear with the loss of vortex mobility, but then reappear. We find that the vortex state can be regarded as an inhomogeneous mixture of a superconducting spin fluid and a material containing a nearly ordered antiferromagnet. These experiments show that as for many other properties of cuprate superconductors, the important underlying microscopic forces are magnetic.

Many of the practical applications of type-II superconductors rely on their ability to carry electrical currents without dissipation even in magnetic fields greater than the Meissner field, below which the superconductor excludes magnetic flux entirely. In such high magnetic fields, superconductors are in a mixed state or "vortex lattice," comprising an array of cylindrical inclusions (vortices) of normal material in a superconducting matrix. Vortex lattices have two magnetic aspects. The first is that there are magnetic field gradients due to the inhomogeneous flux penetration; each vortex allows a magnetic flux quantum to penetrate, and the magnetic field

[1]Oak Ridge National Laboratory, Oak Ridge, TN 37831, USA. [2]N.E.C. Research, 4 Independence Way, Princeton, NJ 08540, USA. [3]Department of Condensed Matter Physics and Chemistry, Risø National Laboratory, 4000 Roskilde, Denmark. [4]Department of Advanced Material Science, Graduate School of Frontier Sciences, University of Tokyo, Hongo 7-3-1, Bunkyo-ku, Tokyo 113-8656, Japan. [5]Department of Physics, University of Loughborough, Loughborough, LE11 3TU, UK. [6]Physikalisches Institute, University of Karlsruhe, D-76128 Karlsruhe, Germany.

*To whom correspondence should be addressed. E-mail: gabe@research.nj.nec.com
†Present address: H. H. Wills Physics Laboratory, University of Bristol, Tyndall Avenue, Bristol, BS8 1TL, UK.

decays from the vortex center into the superconductor over a distance of order the London length λ (*1*). λ is the depth beyond which the superconductor excludes small fields and is typically between 100 and 1000 nm. The second aspect is that the electron spins in the nonsuperconducting cores should no longer be paired coherently (as they are in the superconducting state). The length scale for this microscopic magnetic effect is the radius ξ of the Cooper pairs, which underlie the phenomenon of superconductivity. ξ ranges from 100 nm—common for conventional, low transition temperature (T_c) superconductors—down to nearly 1 nm, which is found for the high-T_c copper oxides. Most magnetic measurements of the flux lattice state, including images from neutron diffraction and microscopy of magnetic nanoparticles deposited on samples threaded by vortices, are sensitive primarily to the mesoscopic field gradients characterized by λ (*2*–*5*). Much less is known about the microscopic magnetism of the vortices. The associated spin correlations and dynamics are important because they mirror the internal structure of the vortices and, in superconductors with strong magnetic interactions, they are likely to dominate vortex state energetics and thermodynamics. Thus motivated, we performed an experiment that images the spin correlations in the vortex state of the simplest high-temperature superconductor, $La_{2-x}Sr_xCuO_4$. The key finding is that, in broad agreement with theory (*6*–*8*), the vortex state for our optimally doped sample (x = 0.163, superconducting transition temperature T_c = 38.5 K) has much stronger tendencies toward magnetic order than the normal or the superconducting state.

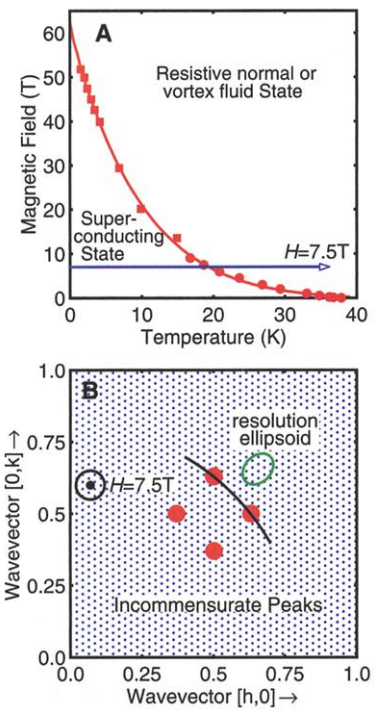

Fig. 1. Phase diagram and wave vector map of $La_{1.837}Sr_{0.163}CuO_4$. (**A**) Red irreversibility line in the *H*-*T* plane, which separates the resistive normal or vortex fluid state from the superconducting state. Red circles come from the magnetotransport measurements (Fig. 4A) and mark the temperatures where nonzero resistivity is first detected for a given field. We also show the data (red squares) of Ando and co-workers (*10*) for a x = 0.17 sample. The blue arrow represents the trajectory of the H = 7.5 T temperature scan (Fig. 4C). (**B**) Reciprocal space for the superconducting CuO_2 planes of $La_{1.837}Sr_{0.163}CuO_4$, as probed by our neutron-scattering measurements. Spin fluctuations are observed at a quartet of incommensurate wave vectors indicated by the red circles. The solid black arc shows the wave vectors measured in a typical constant-energy scan (see Fig. 3), and the green ellipse represents the instrumental resolution. The magnetic field was applied perpendicular to the CuO_2 planes, and the blue dots indicate the reciprocal lattice associated with the H = 7.5 T vortex state.

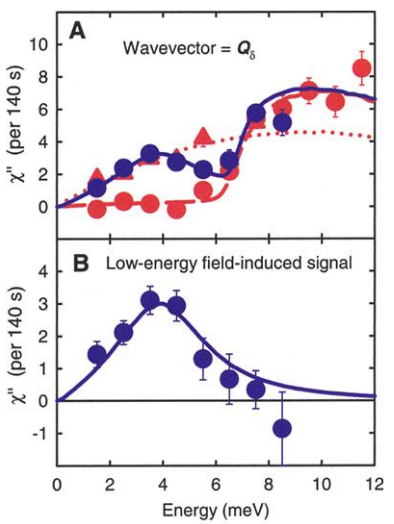

Fig. 2. Constant–wave vector scans plotted as functions of energy. The energy resolution is 0.4 meV full-width-at-half-maximum. (**A**) The magnetic susceptibility χ'' measured at the incommensurate peak $\mathbf{Q}_\delta$, in zero applied field for both the superconducting state (red circles) and the normal state (red triangles). χ'' was also measured in a magnetic field of H = 7.5 T at T = 7.7 K (blue circles). The blue line through the data corresponds to the damped harmonic oscillator $E_o^2E\gamma/((E^2 - E_o^2)^2 + E^2\gamma^2)$ (with E_o = 4.3 ± 0.5 meV and γ = 4.3 ± 0.2 meV), which models the magnetism of the vortices, plus the gapped form described in (*15*), to account for the remaining superconducting signal. The dashed red line is the form from (*15*) alone and describes the gapped spin-fluid–like response of the superconductor at H = 0 T. The dotted red line is the quasi-elastic response $E\Gamma/(E^2 + \Gamma^2)$ (with Γ = 9 meV), which was used previously to account for the normal state signal (*15*). (**B**) The difference between the H = 7.5 T and H = 0 results at low T. The solid blue line is the difference between the blue and dashed red lines in (A).

We used inelastic neutron scattering to measure χ'' (the Fourier transform of the two-spin correlations divided by the Bose factor) as a function of momentum and energy. The superconducting CuO_2 planes of our sample were placed in the horizontal scattering plane of a neutron-scattering spectrometer, and the magnetic field H was applied perpendicular to these planes in the vertical direction (*9*). A sliver of one crystal was used for magnetotransport measurements, and these measurements were combined with earlier data for x = 0.17 (*10*) to establish the *H*-*T* phase diagram (Fig. 1A). The electrical resistance vanishes below an irreversibility line (*11*), which is a very rapid function of applied field, so that even for fields well below the upper critical field H_{c2} (defined here as the field at which nonzero resistivity is first detected), the vortex lattice required for macroscopic superconducting phase coherence and perfect conductivity does not occur until T is well below $T_c(H = 0)$ = 38.5 K, the zero-field transition temperature.

$La_{1.837}Sr_{0.163}CuO_4$ displays spin fluctuations peaked at a quartet of x-dependent characteristic wave vectors given by $\mathbf{Q}_\delta = (\frac{1}{2}(1 \pm \delta), \frac{1}{2})$ and $(\frac{1}{2}, \frac{1}{2}(1 \pm \delta))$ with δ = 0.254 (*12*, *13*) (Fig. 1B). Superconductivity has several effects on the magnetic fluctuations, the most pronounced of which is that an energy gap, Δ, appears in the spectrum (*14*, *15*) (Fig. 2A). On cooling from T_c = 38.5 K to 5.5 K in zero field, the normal state continuum is eliminated below Δ = 6.7 meV. Application of a 7.5-T field fills the gap at base temperature with a spectrum whose amplitude is little different from that seen in the same energy range in zero field at T_c. This means that the vortex state for a field far below the upper critical field $H_{c2} \approx 62$ T (*10*), where the vortex cores presumably occupy a small volume fraction of the material (H/H_{c2} = 12%), displays low-frequency magnetic fluctuations of roughly the same strength as the ungapped normal state. The difference plot (Fig. 2B) shows that the field-induced signal peaks at 4.3 ± 0.5 meV and decays to zero as E approaches either 0 or Δ. This characteristic energy is approximately half that of the normal state, indicating that the fluctuations in the field are two times slower and manifest a greater tendency toward antiferromagnetic order.

To understand the spatial nature of the field-induced sub-gap fluctuations, we performed scans for fixed energy transfer as a function of wave vector along the solid black trajectory (Fig. 1B). At low temperatures and energies below the gap (T = 6.6 K, E = 2.5 meV), a field of H = 7.5 T (Fig. 3A) induces sharp peaks at the same wave vectors where the normal state response is maximal (Fig.

3B). We also investigated the magnetic correlations just above the spin gap at 7.5 meV and find that the field has no discernible effect on the magnetic correlations at this energy (Fig. 3, C and D).

Closer examination of Fig. 3, A through D, yields a wealth of quantitative information about the microscopic magnetism of the vortex state. First, the preferred periodicity, derived from the peak positions $\boldsymbol{Q}_\delta$ of the magnetization density, is $2/\delta = (7.86 \pm 0.18)a_0$, where $a_0 = 3.777$ Å is the Cu^{2+}-Cu^{2+} separation. This value is indistinguishable from the periodicity found for the normal state. Second, the scattering profile is slightly different from that measured at 38.5 K for $H = 0$, in that the peaks seem sharper in the vortex state even though the scattering between the peaks has the same amplitude when scaled to the peaks. Indeed, the peaks are as sharp as the instrumental resolution permits, implying that the principal (period $2/\delta$) magnetization oscillations in the vortex state are coherent over distances $l_v > 20a_0$, to be contrasted with distances $l_n = (6.32 \pm 0.22)a_0$ for the normal state (*15*). For comparison, the lattice constant for a well-formed (Abrikosov) vortex state is $a_V = (2\Phi_0/\sqrt{3}H)^{1/2}$, where the magnetic flux quantum $\Phi_0 = 2067$ T(nm)^2. At 7.5 T, $a_V = 47.2a_0$, a number much larger than $2/\delta$ but potentially similar to l_v.

We also measured the temperature dependence of the field-induced response. Figure 4 shows electrical resistivity as well as neutron data, collected with wave vector and energy fixed at $\boldsymbol{Q}_\delta$ and 2.5 meV, respectively. At $H = 0$, the neutron signal undergoes a sharp drop starting at T_c (Fig. 4C) [which is where the transition to zero resistance also occurs (Fig. 4A)], and dwindles into the background below 15 K. A field of $H = 7.5$ T has a large effect on the temperature evolutions of both the resistivity and the neutron intensity. The resistivity descends steadily as temperature decreases between T_c and 30 K (Fig. 4A) and does not have its final inflection point, as measured by $d\rho_{ab}/dT$ (Fig. 4B), until 25K, which is also where irreversibility sets in. This inflection point has been found (*16*) to coincide with the drop in the magnetization associated with the freezing transition of vortices; above the freezing point, the imposed current loses energy via vortex motion, whereas below, the vortices are pinned and the current is dissipationless. The corresponding magnetic neutron scattering signal (Fig. 4C), which is slightly suppressed at $T > T_c$, remains close to its normal state value for $T_c > T > 25$ K, and undergoes a sharp decline below 25 K. Thus, our spin signal, a microscopic probe of vortices, tracks a macroscopic measure—namely the electrical resistance—of vortex freezing (*17*).

How can our microscopic results be connected to the bulk data? In the vortex fluid state for $T > 25$ K, all Cu^{2+} sites are visited occasionally by vortices, which then depart. While at the sites, the vortices establish a decaying (in time) magnetization density wave, the quantity to which our experiment is sensitive. Thus, all Cu^{2+} sites would have some memory of visits by vortices. When the inverse residence time τ^{-1} of a vortex at any site approaches the frequency of the measured spin fluctuations, the fraction of sites with such memory will begin to significantly exceed the fraction H/H_{c2} of sites covered by vortices at a given instant. The resistivity data in Fig. 4A yield the crude estimate of 2.5 meV for $\hbar\tau^{-1}$ at 30 K (*18*), which happens to coincide with $\hbar\omega$ in Fig. 4C. As T is cooled below 25 K, the vortices become pinned via a combination of their mutual interactions and intrinsic disorder, such that they are always present at certain sites and never present at others. The outcome is then that sub-gap magnetization fluctuations occur only near the relatively small fraction of sites where vortices are pinned and the magnetic response is correspondingly reduced.

Although observing vortex freezing via the electron spin correlations is unprecedented, an even more fascinating phenomenon occurs below 10 K. Here, the decline of the signal below the freezing transition is reversed, resulting in a susceptibility equal to the normal state χ''. Macroscopic measurements (*10*) do not indicate any changes

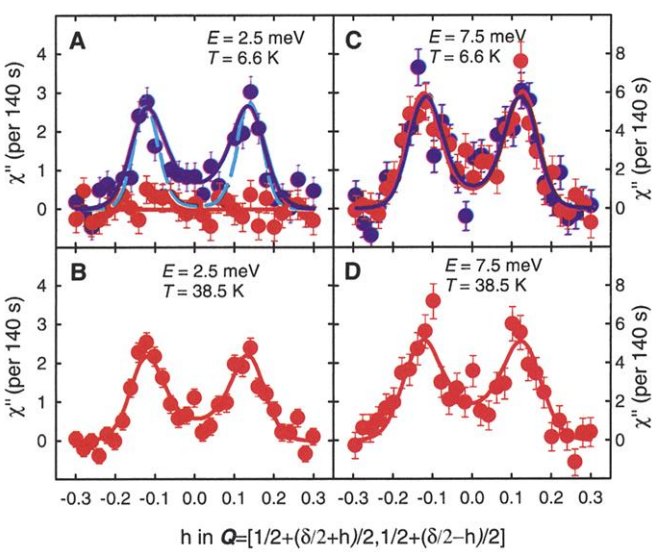

Fig. 3. Constant-energy scans plotted as a function of wave vector along the black trajectory shown in Fig. 1B. (**A**) The susceptibility measured for $T = 6.6$ K, below the energy gap. The data are sums of scans for $E = 1.5$, 2.5, and 3.5 meV. In zero field (red circles) the susceptibility is completely suppressed by superconductivity and application of a 7.5 T field (blue circles) induces a sub-gap signal. For comparison, the normal state susceptibility is shown in (**B**). (**C** and **D**) The susceptibility above the energy gap at $E = 7.5$ meV in both the normal and superconducting states, respectively. The lines in all frames except (A) are the resolution-corrected Sato-Maki lineshape (*32*); for $H = 0$, the width parameters were fixed at the values established from the higher resolution data of (*15*). The solid blue line in (A) is the fit to the normal state data from (B), scaled to match the peak amplitudes, whereas the dashed blue line consists of two resolution-limited peaks. The red line in (A) is zero.

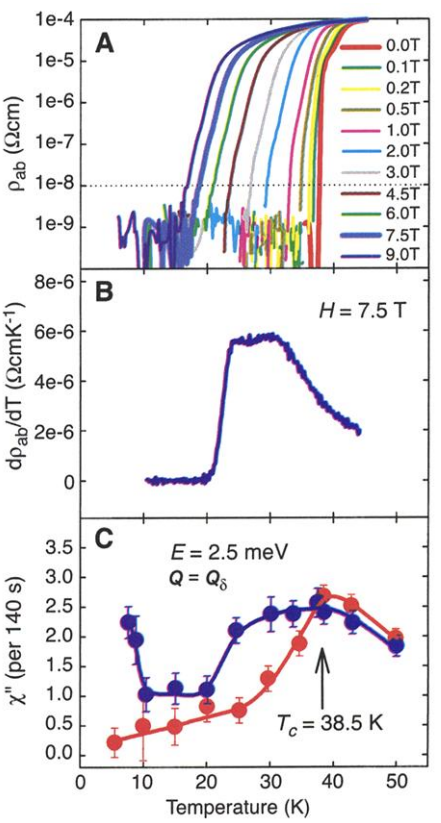

Fig. 4. Temperature-dependent electrical transport and neutron data. (**A**) The in-plane resistivity data collected at a variety of fields from $H = 0$ to 9 T. (**B**) The derivative of the in-plane resistivity with respect to temperature at $H = 7.5$ T, which is the field used in the neutron-scattering experiment. (**C**) The magnetic susceptibilities χ'' at $\boldsymbol{Q} = \boldsymbol{Q}_\delta$ and below the energy gap at $E = 2.5$ meV, for $H = 0$ T (red circles) and $H = 7.5$ T (blue circles).

in the vortex order or dynamics. Therefore, whereas they can plausibly account for the abruptly falling signal near 25 K, such changes cannot be responsible for the rising signal below 10 K. We conclude that the low T increase can only follow from changes in the magnetism of the frozen vortex matter, and we speculate that its most likely cause cannot be the relatively large magnetic interactions we suspect exist within individual vortices, but rather the weaker interactions between spins in different vortices that become relevant only at low T.

Our data show that a modest field induces extraordinary sub-gap excitations in the optimally doped high-T_c superconductor $La_{1.837}Sr_{0.163}CuO_4$. There are several possible origins for such excitations. The first are the quasiparticles inhabiting the vortex cores, which in conventional superconductors are simply metallic tubes with finite-size quantization of electron orbits perpendicular to the tube axes (*19*, *20*). The second, thought to be responsible for the $\sqrt{H}$ low T specific heat in d-wave superconductors, is due to the nodal quasiparticles whose energies are Doppler-shifted by the supercurrents around the vortices (*21*). The third is that the cores are small antiferromagnets, but because of finite size quantization and the weak magnetic interactions between planes as well as between vortices within the same planes, the antiferromagnetic correlations are dynamic and are characterized by finite oscillation frequencies and relaxation rates. The quasiparticles of the first possibility are excluded because the signal we measure is comparable to that found in the normal state, giving a superconducting-to-normal state signal ratio, which is much larger than the volume fraction H/H_{c2} occupied by vortices in such models. The second possible origin has an analogous difficulty with the low T-specific heat C, which does appear to follow the d-wave prescription for our samples (*22*). The ratio of the low temperature (for 7.5 T) and paramagnetic phase Sommerfeld constants C/T is 15%, much less than the 100% ratio of field-induced low T–to–zero-field paramagnetic signals measured with the neutrons. This leaves us with the third option in which we imagine the vortex state not only as an inhomogeneous mixture of paramagnetic and superconducting regions, but as a magnetically inhomogeneous mixture as well. The superconducting regions have a well-defined spin gap, whereas the paramagnetic regions contain fluctuations toward long-period magnetic order. This option better accounts for the observed sub-gap spectral weight than the other two scenarios. Specifically, we estimate that the net sub-gap weight [placed in absolute units using normalization to phonon scattering (*23*)] integrated over energy and reciprocal space corresponds to $0.05\mu_B^2/Cu^{2+}$, which is remarkably close to $H/H_{c2}\mu^2_{2D,S=1/2} = 0.044\mu_B^2$, the product of the volume fraction occupied by the vortices and the square of the ordered moment $\mu_{2_{D,S=1/2}} = 0.6\mu_B$ found in insulating two-dimensional $S = 1/2$ Heisenberg antiferromagnets (*24*). In other words, the ordered moment that for the model insulator appears as an elastic Bragg peak, becomes a fluctuating moment manifested in the inelastic sub-gap peak for the vortex state of the superconductor.

Although the simple picture of inclusions of finite-size vortices with large spin density wave susceptibilities accounts for many of our observations, the material in a field cannot be simply visualized as a superconductor perforated by an array of independent, nearly antiferromagnetic cylinders with diameter given by the pair coherence length. First, the spin density period is of the order of the pair coherence length ξ, and the magnetic correlation length is substantially longer than ξ. Second, the magnetic field also induces broad scattering between the incommensurate peaks with a characteristic length scale of the order $a_0 \ll \xi$. Third, as described above, the low T rise in χ'' is difficult to explain without invoking weak interactions between the spins in "separate" vortices. The observations together show that the spins in the vortices are correlated over a variety of length scales from the atomic to the mesoscopic. The most natural explanation is that the vortices themselves are highly anisotropic objects, or, at the very least, have a highly anisotropic effect on the spin correlations in the intervening superconducting regions. Such anisotropy is consistent with a d-wave pairing state, although it has not been detected in scanning probe images of vortices of high-T_c superconductors (*25*, *26*).

We have measured the microscopic spin correlations associated with the vortex state in the optimally doped single-layer high-T_c cuprate $La_{1.84}Sr_{0.16}CuO_4$. We found that on cooling in a modest field, low-energy spin fluctuations are suppressed not near the zero-field transition but at the irreversibility line below which the superconductor is in a true zero resistance state. This links the development of the spin gap more to superconducting phase coherence—required for zero electrical resistance—throughout the sample than to local pairing. A second discovery is that at low temperatures, the vortex matter exhibits a rising tendency toward the magnetic order found for the "striped" state (*27*–*29*) with $x = 1/8$. This implies that in the H-T plane, the critical line separating frozen from fluid-like "vortex" states may actually mark mesoscopic phase separation—or "gellation"—into a nearly magnetic vortex network bathed in a superconducting quantum spin fluid.

References and Notes

1. C. Kittel, *Introduction to Solid State Physics* (Wiley, New York, ed. 3, 1986), pp. 319–358.
2. S. J. Bending, *Adv. Phys.* **48**, 449 (1999).
3. L. F. Cohen, H. J. Jensen, *Rep. Prog. Phys.* **60**, 1581 (1997).
4. B. Pannetier, A. Bezryadin, A. Eichenberger, *Physica B* **222**, 253 (1996).
5. E. M. Forgan *et al.*, *Physica C* **185**, 247 (1991).
6. D. P. Arovas, A. J. Berlinsky, C. Kallin, S. C. Zhang, *Phys. Rev. Lett.* **79**, 2871 (1997).
7. J. H. Han, D.-H. Lee, e-Print available at http://xxx.lanl.gov/abs/cond-mat/0003222.
8. M. Franz, Z. Tesanovic, e-Print available at http://xxx.lanl.gov/abs/cond-mat/0002137.
9. The single crystal samples were described previously (*15*), and 11 of them (with a total weight of 25 g) were mutually aligned to within ±0.6 and ±3.9 degrees in directions parallel and perpendicular to the CuO_2 basal planes, respectively. The resulting sample was placed on the cold finger of a variable temperature insert in a split coil superconducting magnet, which in turn was installed on the sample table of the RITA (TAS6) cold neutron spectrometer at DR3, Risø National Laboratory (*30*, *31*).
10. Y. Ando *et al.*, *Phys. Rev. B* **60**, 12475 (1999).
11. P. L. Gammel, L. F. Schmeeyer, J. V. Waszczak, D. J. Bishop, *Phys. Rev. Lett.* **61**, 1666 (1988).
12. S-W. Cheong *et al.*, *Phys. Rev. Lett.* **67**, 1791 (1991).
13. K. Yamada *et al.*, *Phys. Rev. B* **57**, 6165 (1998).
14. K. Yamada *et al.*, *Phys. Rev. Lett.* **75**, 1626 (1995).
15. B. Lake *et al.*, *Nature* **400**, 43 (1999).
16. T. Sasagawa *et al.*, *Phys. Rev. B* **61**, 1610 (2000).
17. G. Blumberg, M. Kang, M. V. Klein, *Phys. Rev. Lett.* **78**, 2461 (1997). These authors found rather different behavior in light scattered by a cuprate superconductor in a magnetic field—a gap-like signature in this charge (rather than spin) spectroscopy persists above the irreversibility line into the vortex fluid state. The relation between the field-induced changes discovered by P. Dai *et al.* [*Nature* **406**, 965 (2000)] for the magnetic "resonance" peak of the bilayer cuprate $YBa_2Cu_3O_{6.6}$ and vortex lattice melting remains to be determined.
18. J. Bardeen, M. J. Stephen, *Phys. Rev. A* **140**, 1197 (1965).
19. C. Caroli, P. G. de Gennes, J. Matricon, *Phys. Lett.* **9**, 307 (1964).
20. H. Hess, R. B. Robinson, J. V. Waszczak, *Phys. Rev. Lett.* **64**, 2711 (1990).
21. G. E. Volovik, *JETP Lett.* **58**, 469 (1993).
22. M. Nohara, M. Isshiki, F. Sakai, H. Takagi, *J. Phys. Soc. Jpn.* **68**, 1078 (1999).
23. G. Aeppli *et al.*, *Science* **278**, 1432 (1997).
24. E. Manousakis, *Rev. Mod. Phys.* **63**, 1 (1991).
25. Ch. Renner, B. Revaz, K. Kadowski, I. Maggio-Aprile, Ø. Fischer, *Phys. Rev. Lett.* **80** 3606 (1998).
26. S. H. Pan *et al.*, in preparation; e-Print available at http://xxx.lanl.gov/abs/cond-mat/0005484
27. J. Zaanen, O. Gunnarsson, *Phys. Rev. B* **40** 7391 (1989).
28. J. M. Tranquada *et al.*, *Nature* **375**, 561 (1995).
29. H. Kimura *et al.*, *Phys. Rev. B* **59**, 6517 (1999).
30. K. Lefmann *et al.*, *Physica B* **283**, 343 (2000).
31. K. N. Clausen *et al.*, *Physica B* **241**, 50 (1997).
32. H. Sato, K. Maki, *Int. J. Magnetism* **6**, 183 (1974).

33. We thank P. Gammel, M. Marchevsky, P. Dai, H. Mook, N. P. Ong, S. E. Hayden, H. Rønnow, C. Renner, S. Battacharaya, and P. Hedegård for helpful disussions. Oak Ridge National Laboratory is managed by UT-Battelle, LLC, for the U.S. DOE under contract DE-AC05-000R22725.

30 October 2000; accepted 23 January 2001